Aerodynamic design of a radially-segmented 2-DOF VIGV for suppressing swirl distortion

Zekun Mao [1,*], Hongxin Zhang [1]

[1] Nanjing University of Aeronautics and Astronautics, China.

Abstract. To address the challenges of leading-edge angle of attack mismatch in axial flow compressors under high swirl distortion conditions, this paper proposes a design method for a two-degree-of-freedom (2-DOF) variable-camber inlet guide vane (VIGV) with anti-swirl distortion capabilities. The design features a movable front vane and a fixed rear vane, incorporating a radially segmented independent adjustment mechanism for the front vane to actively match radially non-uniform flow fields. First, based on parametric sweeps using 2D numerical simulations, a geometric design criterion correlating front vane deflection angle with blade chord length was established to determine the critical threshold for suppressing suction-side separation on the rear vane. Subsequently, the three-dimensional aerodynamic performance of the proposed 2-DOF VIGV was compared with a single-DOF design under typical radial swirl distortion inlet conditions. The results demonstrate that, by differentially adjusting the front vane angles at the hub and tip segments, the 2-DOF design reduces the outlet swirl distortion index (SC(60)) by 47.1% and the total pressure loss coefficient by 3.5% compared to the single-DOF baseline, while achieving an outlet flow angle closer to the axial design target. This design effectively mitigates flow separation at large turning angles and significantly enhances the aerodynamic stability and flow uniformity of the compressor under complex inlet distortion conditions.

Keywords: Variable-camber inlet guide vane (VIGV); Two-degree-of-freedom (2-DOF) adjustment; Swirl distortion.

1. Introduction

In the design of modern high-performance aero-engines, in order to match the wide flight envelope and ensure the aerodynamic stability of the propulsion system under variable conditions, variable geometry technology has become one of the core elements of compressor design [1,2]. In particular, the traditional adjustable inlet guide vane technology, which guides the airflow deflection by rotating the entire guide vane, is widely used to control the intake flow by adjusting the pre-swirl, thereby optimizing the operating conditions of the rotor at off-design points. However, when the compressor is operating at a large angle away from the design point, the traditional guide vane faces a severe aerodynamic challenge: in order to generate sufficient pre-swirl, the blade often needs to be greatly deflected, which causes the leading edge of the blade to bear a very high angle of attack. This mismatch of the leading edge angle of attack will induce a strong reverse pressure gradient and boundary layer separation on the suction surface of the blade, which will lead to a sharp increase in the total pressure loss. More seriously, the low-energy fluid generated by the separation will deteriorate the rotor inlet flow field during the downstream transport process, forming a strong swirl distortion with circumferential and radial non-uniformity, which not only weakens the compressor 's flow capacity, but also significantly reduces its surge margin due to periodic aerodynamic load fluctuations.

To alleviate the flow separation issues associated with traditional variable inlet guide vanes at high turning angles, existing research frequently adopts tandem blade designs. A representative configuration is the variable camber guide vane (VIGV) featuring a fixed front vane and a movable rear vane [3]. This configuration induces airflow deflection through the rotation of the rear vane and utilizes the slot effect to delay flow separation on the rear vane. However, in the presence of severe inlet flow distortion, this "fixed front" geometric characteristic becomes a critical bottleneck limiting performance. Under inlet distortion conditions, the fixed front vane is unable to adapt to variations in inflow angle. Consequently, its leading edge remains under adverse conditions of high incidence, which is prone to inducing leading-edge suction spikes and subsequent flow separation.

Once massive separation occurs on the front vane, the resulting wake directly disrupts the flow structure passing through the rear vane, rendering the rear vane incapable of effectively regulating the outlet flow to achieve the intended rectifying effect. Furthermore, although Non-axisymmetric IGV technology [4] has been proven capable of passively counteracting specific inlet distortions through circumferentially non-uniform blade profiling, this design based on fixed geometry struggles to adapt to the complex and varying flow requirements under variable engine operating conditions.

In light of the aforementioned limitations, this paper proposes a design method for a two-degree-of-freedom (2-DOF) variable camber inlet guide vane (VIGV) capable of resisting swirl distortion, and numerically investigates its aerodynamic characteristics. This design innovatively adopts a configuration featuring a movable front vane and a fixed rear vane, while incorporating a radially segmented independent adjustment mechanism for the front vane. Compared with traditional fixed-front designs, by endowing the front vane with rotational degrees of freedom, this method enables active adjustment of the setting angle to match the incoming flow direction across the entire operating range, thereby consistently maintaining the leading-edge incidence within the low-loss boundary layer attachment region [5]. Crucially, considering that inlet swirl distortion is often accompanied by significant radial non-uniformity, the capability for radially independent adjustment of the front vane allows for differential control targeting flow characteristics at different spanwise heights. This 2-DOF adjustment strategy enables more precise correction of radially distinct flow structures, effectively resisting and attenuating complex upstream swirl distortion, and consequently providing a high-quality, highly uniform inlet flow field for the downstream core engine.

2. Text Investigated Geometry and Numerical Methods

2.1 Investigated Geometry

Figure 1(a) illustrates the schematic of the structure and operation process of the 2-DOF VIGV. In this study, the connections between the front and rear parts of the blade, as well as the spanwise transition section, are assumed to be made of perfectly elastic material, ensuring a smooth aerodynamic surface transition during the rotation of the front vane. Additionally, the leakage flow effects caused by the pivot gaps are neglected in the computational model. In practical engineering applications, the independent radial adjustment of the front vane segments can be achieved through a concentric shaft mechanism. Since the flow passage exhibits a contracting shape along the axial direction, all relative radial heights (spans) in this paper are defined based on the height of the blade leading edge (LE) for consistency. The blade features a variable hub-to-tip ratio design, with a value of 0.2892 at the leading edge and 0.3662 at the trailing edge. To address radially non-uniform swirl distortion, the 2-DOF front vane is divided radially into three functional regions: the region near the hub is defined as the hub-segment, covering a radial range of 0%–60% span; the region near the casing is defined as the shroud-segment, covering 70%–100% span; and a spanwise transition section is located between 60% and 70% span to smoothly connect the hub and shroud segment. The pivot axis controlling the front vane's rotation is positioned at the location of maximum blade thickness to balance structural integrity and aerodynamic performance. The key geometric parameters of the mid-span section (50% span) in the initial unrotated state are listed in Table 1.

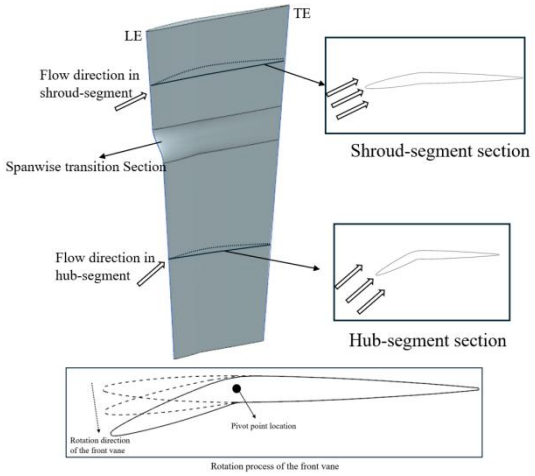

(a) Schematic of the structure and operation process of the 2-DOF VIGV

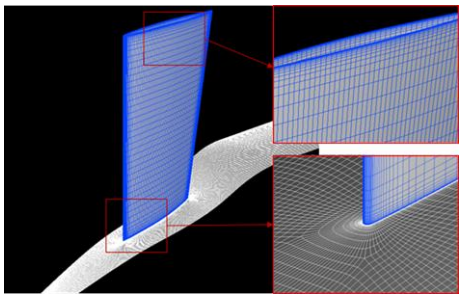

(b) Schematic diagram of 3D VIGV mesh model

Fig. 1 Schematic of the structure and operation process(left), mesh model(right) for the 2-DOF VIGV

Table 1.Geometric parameters of the mid-span section in the initial state

Geometric feature parameters	Value
Chord length(mm)	91.13
Relative position of maximum thickness	0.35
Maximum thickness(mm)	6.3925
Consistency	1.0

2.2 Numerical Method

The three-dimensional steady numerical simulations in this paper were performed using the commercial CFD software NUMECA FINE/Turbo. The computational mesh was generated using the AutoGrid module. An O-type topology was adopted around the blade to ensure grid orthogonality, with refinement applied to the near-wall regions. The height of the first grid layer was set to 0.003 mm to ensure a dimensionless wall distance $y+ < 1$, thereby satisfying the near-wall resolution requirements of the turbulence model (as shown in Fig. 1(b)). The Reynolds-Averaged Navier-Stokes (RANS) equations were solved as the governing equations, with the Spalart-Allmaras (S-A) one-equation model selected for turbulence closure. This model has been verified to accurately predict boundary layer flow characteristics while demonstrating excellent computational convergence and economic efficiency [6].

Regarding the boundary condition settings, the inlet was specified with total temperature, total pressure, and a flow angle distribution generated by a three-dimensional steady swirl distortion program, while static pressure was imposed at the outlet. Across simulations with varying guide vane geometries, the back pressure was adjusted to maintain a constant inlet Mach number of 0.55. For the bulk swirl inflow condition, the computational domain comprised a single blade passage with periodic boundary conditions applied in the circumferential direction. For the 2D calculations, the mid-span blade element was extruded to a radial height of 10% of the leading-edge radial height, with 30 grid layers distributed in the radial direction.

To exclude the influence of grid density on the numerical results, Fig. 3 presents a comparison of the outlet total pressure loss coefficients for the unrotated baseline VIGV using three different grid densities under the inlet swirl distortion conditions illustrated in Fig. 2. Balancing computational accuracy and efficiency, the Medium Grid was selected as the baseline mesh for the subsequent numerical investigations.

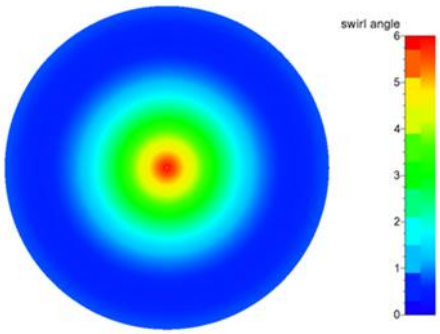

Fig. 2 Swirl angle distribution at the inlet section

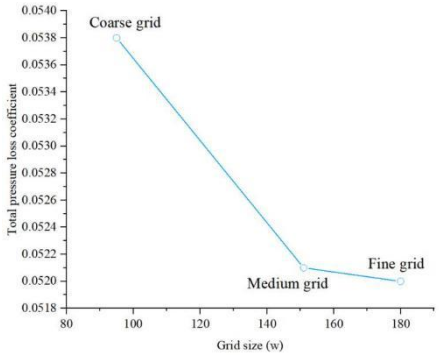

Fig. 3 Total outlet pressure loss coefficients for three different grid schemes

3. Results Analysis and Discussion

3.1 Investigation on Front Vane Deflection Limit and Chord Matching Criterion Based on 2D Simulations

Fig. 4 and 8 demonstrate that the guide vane exhibits excellent active control capability under moderate variations in inflow incidence. By moderately deflecting the front vane to effectively match the incoming flow direction, the leading-edge suction spike is eliminated, thereby maintaining flow attachment. However, this aerodynamic control capability has a physical limit. When an excessive front vane deflection angle θ is required to accommodate high inflow incidence, although leading-edge separation is suppressed, the fluid experiences a severe adverse pressure gradient across the transition region between the front and rear vanes due to the excessive flow turning. Once this adverse pressure gradient exceeds the capacity of the suction surface boundary layer, massive separation occurs on the suction side of the rear vane, leading to a failure of the vane's flow straightening function.

This flow instability induced by large deflection angles essentially reflects a mismatch between the aerodynamic loading (determined by the deflection angle) and the geometric load capacity (determined by the blade chord length). Increasing the total chord length b, and particularly extending the rear vane chord b2, can effectively alleviate the streamwise pressure gradient on the blade surface, thereby delaying the onset of flow separation. Therefore, it is hypothesized that a critical coupling relationship exists between the front vane deflection angle θ and the blade chord length b. When a function of these two parameters exceeds a specific threshold, massive separation inevitably occurs on the suction side of the rear vane.

To quantitatively reveal this geometric constraint and establish design criteria, a parametric sweep over a wide range of "deflection-chord" combinations is required. Given the prohibitive computational cost and time associated with 3D full-annulus simulations, and considering that profile separation characteristics are primarily governed by the two-dimensional aerodynamic parameters of the blade section, a 2D numerical approach is adopted in this section. Through extensive calculations on mid-span blade elements, the objective is to construct a dimensionless criterion function correlating the front vane deflection angle with the chord length at a low computational cost. This criterion provides rapid and reliable geometric constraint guidance for the subsequent 3D anti-distortion design, thereby avoiding computationally expensive trial-and-error in 3D simulations.

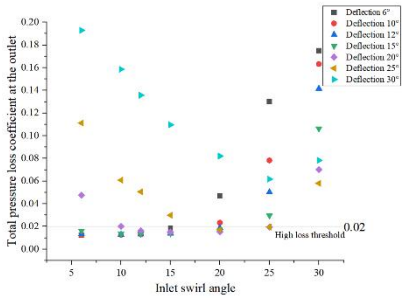

Fig. 4 Variation of total pressure loss coefficient with inlet swirl angle at different front vane deflections

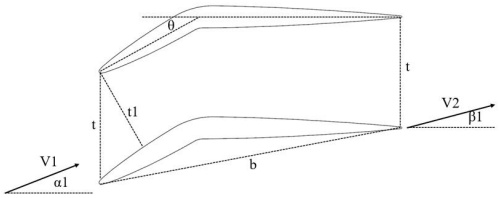

Fig. 5 Schematic diagram of 2-D VIGV

According to two-dimensional cascade loss theory, the primary cause of profile loss in a blade element is directly correlated with the wake momentum thickness of the blade surface boundary layer. The boundary layer thickness, in turn, is closely related to the degree of diffusion on the blade surface, and its magnitude is directly proportional to the diffusion on the suction surface at the minimum loss condition. Based on the two-dimensional incompressible turbulent boundary layer theory, Lieblein [7] proposed the Diffusion Factor (D-factor) to evaluate the aerodynamic loading level of compressor cascades. Subsequently, the D-factor has been widely developed and validated [8]. Figure 5 illustrates the schematic of the flow passage for the VIGV investigated in this study. Analogous to the diffusing passage in compressor cascades, the equivalent flow area of the VIGV front vane is smaller than that of the rear vane, resulting in an overall deceleration and diffusion process, which shares certain similarities with compressor cascades. Therefore, the D-factor is adopted in this paper to evaluate the loading level of the VIGV. The expression for the stator D-factor is as follows:

$$D = 1.0 - \frac{V_2}{V_1} + \frac{\Delta V_t}{2\tau V_1} \tag{1}$$

In the preliminary design phase, it is assumed that the direction of the rear vane outlet velocity is parallel to the axial direction (i.e.,β1=0). Here, only the condition of 0° relative incidence is analyzed, meaning $\alpha_1 = \theta$. Furthermore, based on the continuity equation and neglecting the influence of blade thickness variation, the diffusion factor D can be finally simplified to the following expression:

$$D = 1.0 - \mathrm{Cos}\theta + \frac{t\mathrm{Sin}\theta}{2b} \tag{2}$$

The simplified VIGV diffusion factor D is solely dependent on the front vane deflection angle θ, the pitch t, and the blade chord length b. With an increase in the front vane deflection angle θ and pitch t, or a decrease in the blade chord length b, the diffusion factor D increases, corresponding to a higher cascade loading level and consequently greater losses within the passage. The formula for calculating the chord length b after the deflection of the front vane is given by:

$$b = \sqrt{a^2 + b_2^2 - 2ab_2\mathrm{Cos}(180 - \theta)} \tag{3}$$

where a and b2 represent the chord lengths of the front and rear vanes, respectively.

Although the outlet total pressure loss coefficient serves as a direct metric for evaluating the operating status and design level of the VIGV, the magnitude of friction loss over the entire blade varies with different rear vane chord lengths and front vane deflection angles. To minimize the influence of blade surface friction losses associated with different airfoil profiles, and referring to Lieblein's study [7] on the relationship between the total pressure loss coefficient and the diffusion factor for NACA-65 airfoils at minimum loss incidence, the total pressure loss parameter $coef_w$ is adopted in this paper:

$$coef_w = \frac{w\mathrm{Cos}\theta}{2\tau} \tag{4}$$

The aerodynamic losses for different airfoil shapes were normalized and represented.

Fig. 6 presents the relationship between the total pressure loss parameter $coef_w$ and the front vane deflection angle θ for airfoils with rear vane chord lengths b2 of 0.5909, 1.0, and 1.3 times the original rear vane chord, respectively. The black dashed lines represent the isolines of the corresponding diffusion factor D. For the three airfoil profiles with different rear vane chord lengths, both the diffusion factor D and the total pressure loss parameter $coef_w$ exhibit an increasing trend with the increase of the front vane deflection angle θ. The increase in $coef_w$ is characterized by two distinct stages: a gradual increase followed by a rapid increase. The transition point between these two stages is located at the threshold point where the diffusion factor D=0.31 for each airfoil. Furthermore, with the increase of the rear vane chord length, this transition point shifts towards larger airflow angles. This preliminarily indicates that an airfoil with a larger rear vane chord length possesses a wider applicable range of inlet airflow angles.

The parameter $coef_w$ exhibits two distinct development stages due to a shift in the underlying flow mechanism. Figure 8 presents the axial velocity contours within the cascade passage for the airfoil with 1.0 times the original rear vane chord length at front vane deflection angles of 20°, 25°, 27.5°, and 30°. In these contours, uncolored regions indicate areas where the axial velocity is negative, and the flow separation boundaries are delineated by red dashed lines. Figure 7 illustrates the variation trend of the relative length of the separation zone on the rear vane suction surface (defined as the ratio of the separation zone length to the rear vane chord length) with respect to the front vane deflection angle. Figure 12 depicts the variations of inlet and outlet airflow angles against the front vane deflection angle for airfoil schemes with different rear vane solidities.

When the front vane deflection angle is small, no flow separation occurs on the entire suction surface of the rear vane. However, as θ increases, the boundary layer at the trailing edge of the rear vane thickens significantly. This deteriorated flow condition restricts the airflow deflection capability of the variable-camber guide vane to a certain extent and simultaneously acts as a precursor to flow separation on the rear vane suction surface. When the front vane deflection angle increases further, causing the diffusion factor D to approach the threshold of 0.31, the boundary layer on the rear vane suction surface reaches a critical state. At this juncture, flow separation is imminent, and the VIGV outlet deviation angle enters a phase of rapid increase. As the front vane deflection angle continues to increase until D=0.35, the separation rapidly propagates over the entire suction surface, signifying the occurrence of open separation on the rear vane surface. With any further increase in the front vane deflection angle, the axial extent of the separation zone remains constant, while the circumferential extent expands further, resulting in greater passage blockage caused by the recirculation.

For the three rear vane solidities investigated, the diffusion factor D corresponding to the onset of the rapid growth phase of $coef_w$ is approximately 0.31. Consequently, a preliminary relationship between the front vane deflection angle θ and the rear vane chord length b2 for ensuring low-loss conditions is derived as follows:

$$D = 1.0 - Cos\theta + \frac{tSin\theta}{2b} < 0.31$$
$$b > \frac{tSin\theta}{2(Cos\theta - 0.69)} \quad (5)$$

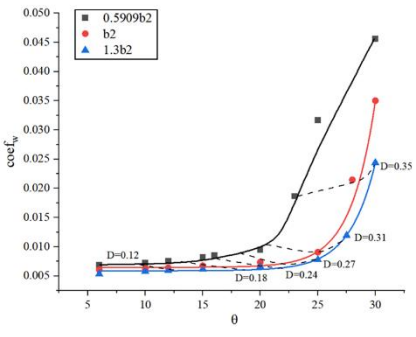

Fig. 6 The relationship for three different posterior leaf chord lengths

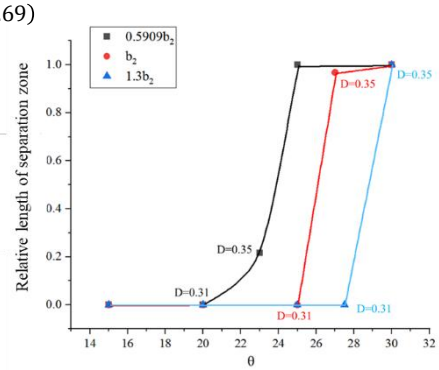

Fig. 7 Relative length of separation

between $coef_w$ and θ region extracted from three types of rear vane

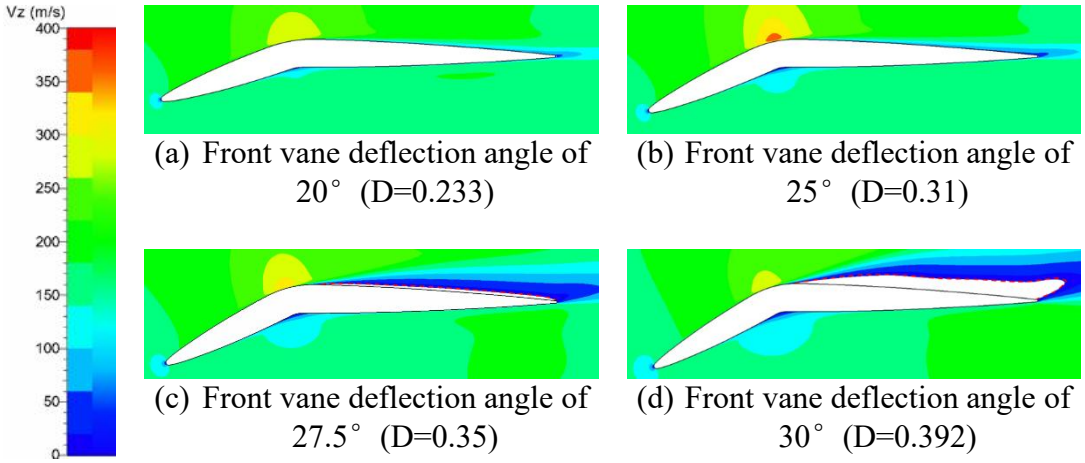

(a) Front vane deflection angle of 20° (D=0.233)

(b) Front vane deflection angle of 25° (D=0.31)

(c) Front vane deflection angle of 27.5° (D=0.35)

(d) Front vane deflection angle of 30° (D=0.392)

Fig. 8 Axial velocity contours at four different front vane deflection angles (Solidity = 1)

3.2 Investigation on Front Vane Deflection Limit and Chord Matching Criterion Based on 2D Simulations

To validate the advantages of the two-degree-of-freedom (2-DOF) design in coping with complex flow fields, a typical radially non-uniform swirl distortion is introduced as the inlet boundary condition in this subsection. As shown in Fig. 9(a), at the Aerodynamic Interface Plane (AIP) located 192 mm from the inlet section, the flow field exhibits significant radial stratification characteristics: high-intensity positive swirl exists in the hub region (with swirl angles ranging from approximately 20° to 25°), while the swirl intensity gradually decreases towards the blade tip. The swirl distortion index SC(60) at the AIP section is 0.3071, indicating the presence of severe swirl angle distortion in the flow field, which places high demands on the incidence matching capability of the guide vanes.

Figures 9(b) and (c) present the contours of swirl angle distribution at the guide vane outlet for the Single-DOF scheme (with the entire front vane rotated by 20°) and the 2-DOF scheme (with radially independent adjustment: the shroud-segment rotated by 10° and the hub-segment rotated by 20°), respectively. For the Single-DOF scheme, due to the constraint of rigid rotation of the entire front vane, it is impossible to simultaneously match the high swirl at the hub and the low swirl at the tip. Although this configuration attenuates the inlet swirl to a certain extent, distinct traces of residual swirl remain at the outlet section. Furthermore, significant flow disturbances are observed in the blade wake regions, indicating the presence of local flow separation or enhanced secondary flows at certain spanwise heights caused by incidence mismatch. In contrast, the outlet flow field of the 2-DOF scheme exhibits significant improvement. The contours indicate that the flow angles in the majority of the region are close to 0° . By independently adjusting the rotation angles of the front vane at the hub- and shroud-segments, the 2-DOF guide vane scheme successfully mitigates the radial variations in the inlet flow and suppresses the downstream transfer of residual swirl.

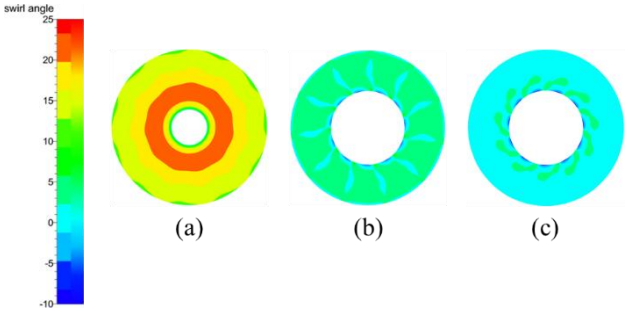

Fig. 9 Contours of swirl angle distribution at (a) the AIP section, (b) the outlet of the Single-DOF VIGV, and (c) the outlet of the 2-DOF VIGV under radial swirl distortion.

Table 2. Comparison of aerodynamic performance parameters of the two VIGV schemes

	Single-DOF VIGV	2-DOF VIGV
AIP SC(60)	0.3071	0.3071
Outlet SC(60)	0.04619	0.02446
w	0.05431	0.05239
Average airflow angle at the outlet	1.394°	2.62°

Table 2 summarizes the comparison of aerodynamic performance parameters for the two VIGV schemes. The data indicate that the 2-DOF design outperforms the Single-DOF scheme across all metrics: the outlet SC(60) of the 2-DOF scheme is reduced to 0.02446, representing a 47.1% reduction compared to the Single-DOF scheme (0.0462). This implies that the capability of the 2-DOF guide vane to attenuate inlet swirl distortion is nearly doubled, providing a more uniform inlet environment for the downstream rotor.

4. Summary

1.A geometric matching criterion based on the "movable front vane, fixed rear vane" configuration was established. 2D parametric studies revealed a critical correlation between the front vane deflection angle and the total chord length. Adhering to this criterion effectively suppresses massive separation on the suction side of the rear vane under large deflection angles, providing a reliable constraint for 3D blade design.

2.The 2-DOF adjustment mechanism significantly enhances the vane's anti-distortion capability. Under severe radial swirl distortion inlet conditions, by independently adjusting the hub and tip segments of the front vane, the 2-DOF design achieves precise matching of radially non-uniform incidence angles. Compared to the single-DOF baseline with rigid rotation, the proposed design reduces the outlet swirl distortion index SC(60) from 0.0462 to 0.02446, a reduction of 47.1%.

References

[1] AN Guangfeng, ZHOU Rui, YU Xianjun, et al. Impact of adjustable stator on flow capacity of variable cycle split fans at low and middle rotating speed[J]. Journal of Propulsion Technology, 2024 (Online First).

[2] MOHSENI A, GOLDHAHN E, VAN DEN BRAEMBUSSCHE R A, et al. Novel IGV designs for centrifugal compressors and their interaction with the impeller[J]. Journal of Turbomachinery, 2012, 134(2): 021006.

[3] YU Xianjun, YANG Mingyu, AN Guangfeng, et al. Investigation of the characteristics of variable tandem stator and its influence on the performance of fan[J]. Journal of Engineering Thermophysics, 2024, 45(3): 697-706.

[4] LIU L, VO H D. Attenuation of inlet distortion effects on fans using asymmetric inlet guide vanes[J]. ASME Journal of Turbomachinery, 2024, 146(10): 101006.

[5] SHI H, LIU B, YU X. Criteria for designing low-loss and wide operation range variable inlet guide vanes[J]. Aerospace Science and Technology, 2018, 80: 177-191.

[6] WANG Jiale, CHENG Bangqin, ZHANG Lei, et al. Effect of specific vortex swirl distortion on performance of transonic compressor[J]. Journal of Aerospace Power, 2020, 35(3): 540-551.

[7] LIEBLEIN S, SCHWENK F C, BRODERICK R L. Diffusion factor for estimating losses and limiting blade loadings in axial-flow-compressor blade elements[R]. Washington, D.C.: NACA, 1953.

[8] GUI Xingmin, et al. Aerothermodynamic theory and application of aero-compressor[M]. Beijing: Shanghai Jiao Tong University Press, 2014.